Estimating the wall-shear stress after a rough-to-smooth step-change in turbulent boundary layers using near-wall PIV/PTV experiments

C. M. de Silva[1,*], M. L. Mogeng[1], R. Baidya[1], A. Rouhi[1], D. Chung[1], I. Marusic[1] and N. Hutchins[1]

1: Department of Mechanical Engineering, University of Melbourne, Victoria 3010, AUSTRALIA.
* correspondent author: desilvac@unimelb.edu.au

ABSTRACT

In this work, we examine the efficacy of near-wall PIV / PTV experiments to estimate the wall-shear stress, after a step change from a rough-to-smooth walled surface in a turbulent boundary layer. To this end, a collection of experimental databases at $Re_\tau \approx 3500$ are captured that have access to either 'direct' or 'indirect' measures of the wall shear stress after a sudden change in surface conditions. Our results reveal that the viscous region recovers almost immediately to an equilibrium state to the new wall conditions, and thus provides a good estimate of the wall-shear stress immediately after the transition. On the other hand, the magnitude of the wall shear stress is consistently underestimated from techniques that use velocity signals further away from the wall. We conclude that techniques such as the high-magnification near-wall particle tracking velocimetry measurements are more suited to measuring the wall shear stress after a sudden change in surface conditions, as compared to more established techniques that rely on assumed velocity profiles further from the wall (Clauser technique, Preston tubes etc).

1. Introduction

Turbulent wall-bounded flows over a change in the surface roughness are commonly observed in engineering applications and meteorology measurements, such as on the hull of a ship with patches of biofouling roughness or in the atmospheric boundary layer over a varying terrain. One such scenario is a sudden transition from a rough-to-smooth walled surface occurring in the streamwise direction as examined in the seminal work of Antonia and Luxton (1972). The configuration is illustrated in figure 1, where upstream of the transition from a rough-to-smooth surface at $\hat{x} = x_0$, an equilibrium rough wall boundary layer has developed over the rough fetch. Following the transition, the new smooth wall condition initially modifies the near-wall region, which then gradually propagates to the interior of the flow further away from the wall with increasing distance downstream of the transition. The layer that separates these two regions is generally referred to as the internal boundary layer (IBL) with a thickness denoted by δ_i (Garratt, 1990).

Although the rough-to-smooth heterogeneity in surface conditions has been studied extensively over the past few decades ((Bradley, 1968; Antonia and Luxton, 1972; Shir, 1972; Rao et al., 1974; Chamorro and Porté-Agel, 2009; Hanson and Ganapathisubramani, 2016)), to date, the recovery to equilibrium conditions to the new wall conditions after such a transition is far from understood. In particular, these attempts have been hampered by reliability

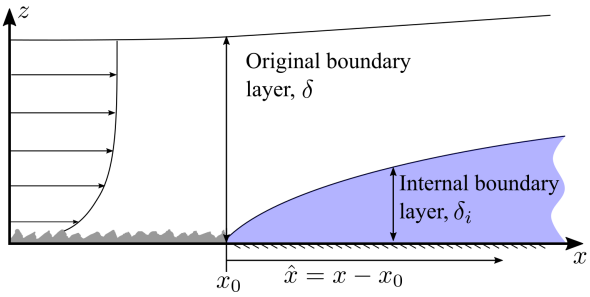

Figure 1: Schematic of a turbulent boundary layer flow over a rough-to-smooth change in surface condition. Flow is from left to right and $\hat{x} = x - x_0$ represents the fetch measured from the rough-to-smooth transition which occurs at $x = x_0$.

issues in determining the local wall-shear stress τ_w after the transition as it provides the friction velocity $U_\tau = \sqrt{\tau_w/\rho}$ for viscous scaling (where ρ denotes density).

1.1 Methods to measure wall-shear stress

The difficulty in obtaining an accurate and reliable measurement of the wall-shear stress τ_w even in a canonical turbulent boundary layer is commonly recognised (Tropea et al., 2007). Techniques to measure τ_w are generally classified as either 'direct' or 'indirect' methods, where measurements of the wall-normal gradient of the mean streamwise velocity ($\mathrm{d}\overline{U}/\mathrm{d}z$) are made directly at the surface or estimates are inferred from data further away from the wall through a set of assumptions, respectively. Particle image velocimetry (PIV) has become increasingly popular over the last decade for accurately measuring multi-component, multi-dimensional velocity fields associated with turbulent flows. However, in common configurations, these techniques are known to have limitations in spatial resolution. Thus, they are not typically able to capture the smaller scales prevalent in the flow. Additionally, these techniques frequently lack near-wall information. To overcome these limitations, Kähler et al. (2012) conducted an experiment in which a spatial resolution in the order of microns is achieved using a highly magnified field-of-view (FOV). Following on from this work, de Silva et al. (2014) and others have adopted similar highly magnified FOVs to capture the near-wall region of a turbulent boundary layer. Such an approach has been shown to be well suited to measure τ_w in a canonical smooth-walled turbulent boundary layer, however, is yet to be examined for wall-bounded flows with sudden changes in surface conditions.

Accordingly, this paper presents a systematic study on estimating τ_w after a rough-to-smooth transition using laser diagnostic experimental techniques. Throughout this paper, the coordinate system x, y and z refer to the streamwise, spanwise and wall-normal directions, respectively. Corresponding instantaneous streamwise, spanwise and wall-normal velocities are represented by $\widetilde{U}$, $\widetilde{V}$ and $\widetilde{W}$, respectively, with the corresponding velocity fluctuations given by lower case letters. Overbars indicate spanwise and time-averaged quantities, and the superscript + refers to normalisation by inner scales. For example, we use $l^+ = lU_\tau/\nu$ for length and $\widetilde{U}^+ = \widetilde{U}/U_\tau$ for velocity, where U_τ is the friction velocity and ν is the kinematic viscosity of the fluid.

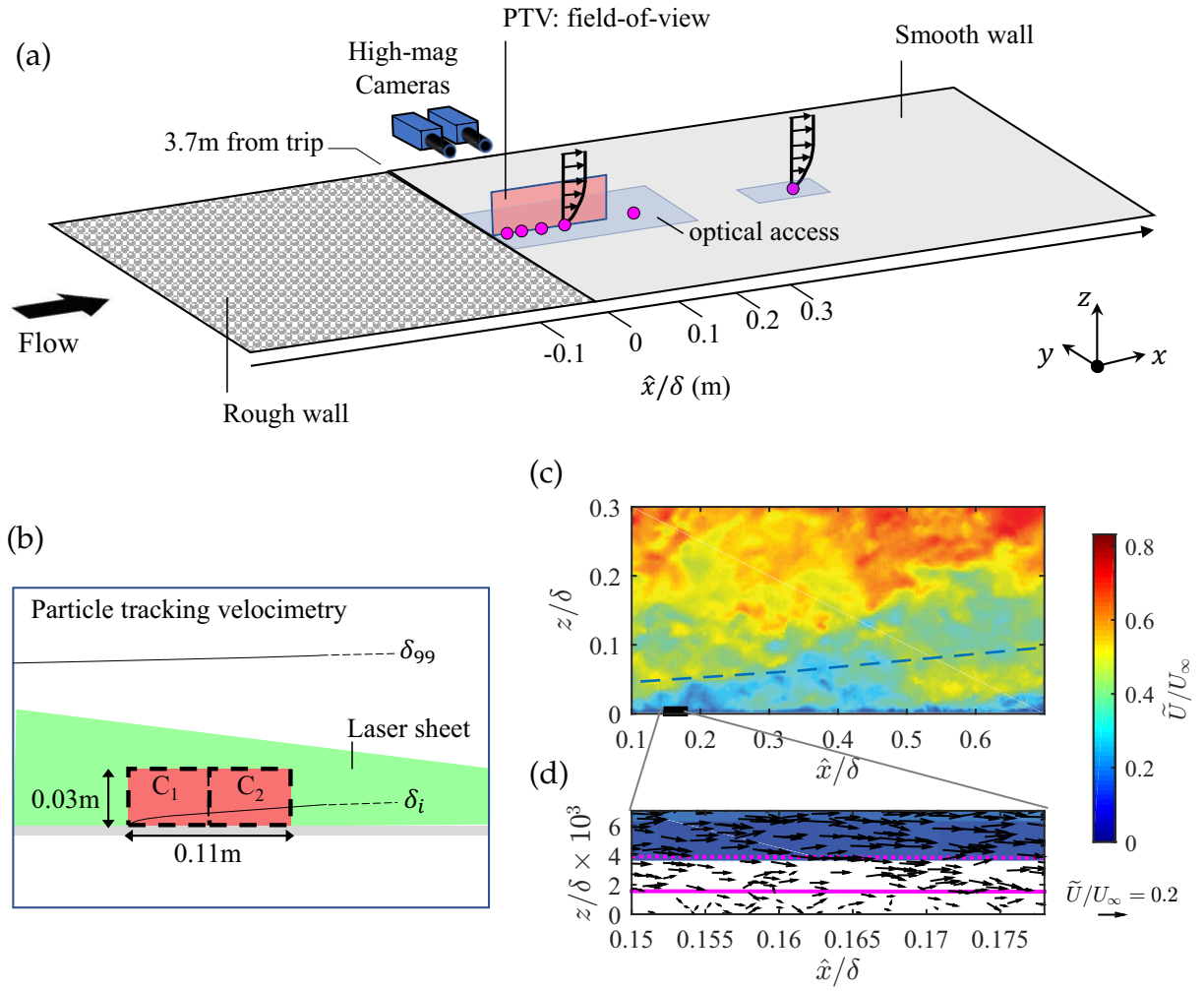

Figure 2: (a) Overview of the experimental campaign in the open-return boundary layer wind tunnel facility at $Re_\tau \approx 3500$. The ● symbols correspond to the locations of the hotwire wall-normal profiles and oil-film interferometry measurements. (b) illustrates the particle tracking velocimetry, where C_1 and C_2 correspond to the field-of-views captured non-simultaneously using a scientific double-frame camera with a vertical laser sheet that is projected upstream through the working section. (c) is an instantaneous field of the streamwise velocity component, $\widetilde{U}$ from the PIV pass. The dashed line marks the location of δ_i. (d) is the enlarged view of the rectangular region in (c). The colour contour is the same as in (c), and the arrows show the velocity vectors from the PTV pass. The solid and dotted magenta lines indicate $z^+ = 4$ and $z^+ = 10$, respectively.

2. Experimental databases

This study utilises a collection of wall-bounded flow databases with a sudden change in surface conditions (rough-to-smooth wall transition). Collectively, the databases have access to both 'direct' and 'indirect' measures of wall-shear stress, and they span several boundary layer thicknesses downstream of the rough-to-smooth transition.

Experiments are performed in an open-return boundary layer wind tunnel facility in the Walter Basset Aerodynamics Laboratory at the University of Melbourne (see Nugroho et al. (2013) and Kevin et al. (2015) for further details). The facility is equipped with a settling

Technique	$\approx Re_\tau$	δ	$\hat{x}/\delta$ range
Hot-wire			$0 < \hat{x}/\delta < 3.5$
Oil-Film	3500	88 mm	$0 < \hat{x}/\delta < 2.0$
PTV			$0 < \hat{x}/\delta < 1.2$

Table 1: Summary of experimental databases. $\hat{x}/\delta$ corresponds to the streamwise extent captured from each measurement downstream of the rough-to-smooth transition at $\hat{x}/\delta = 0$.

chamber, followed by flow conditioning and then a contraction section with an area ratio of 8.9:1. The $6.7 \times 0.94 \times 0.38$ m^3 working section of this facility is topped with an adjustable perspex roof to enable fine pressure gradient adjustment. Further, the test surface (bottom wall) of the working section can be lowered using a hydraulic lift to ease the interchange of the test surface.

The arrangement of the experimental campaign consisting of hot-wire boundary layer traverses, oil film interferometry measurements and PTV measurements are depicted in figure 2. For the present work, the first 3.7 m of the tunnel surface is covered by P16 grit sandpaper, while the remaining streamwise length is a smooth-walled surface. Details of the roughness parameters are obtained by scanning a 60mm × 60mm section of the sandpaper using an in-house laser scanner. To summarise, the average peak height of the roughness elements before the rough-to-smooth transition is approximately 3 mm above the smooth-walled surface, which is approximately 4% of the boundary layer thickness, δ, at $x = x_0$ (the location of the transition).

2.1 Particle tracking velocimetry

In order to resolve the near-wall region, high magnification Particle Tracking Velocimetry (PTV) measurements are performed immediately after the rough-to-smooth transition. The magnified field of view targeted at the near wall region is ideally suited for this analysis, as the database provides access to well-resolved velocity signals within the viscous sublayer region of the flow ($z^+ \lesssim 4$). The imaging system consisted of a 14 bit PCO 4000 PIV camera (4008 × 2672 pixels) equipped with a Tamron 180mm Macro lens and a Sigma APO EX DG 2× teleconverter. This configuration which is illustrated in figure 2(b) provides a FOV of approximately 5.5 cm × 3 cm ($0.62\delta \times 0.34\delta$) per camera with a pixel size of ≈ 12 μm ($0.33\nu/u_\tau$). We note, the high-magnification optics limited the wall-normal extent of the FOV to 0.5δ. However, in order to capture a larger streamwise extent ($\approx 1\delta$), the camera is mounted on a linear traverse, which enables non-simultaneous measurements further downstream of the rough-to-smooth transition. For the present study, two measurement locations are captured as shown in figure 2(b) that span the range $0 \lesssim \hat{x}/\delta \lesssim 1.2$.

Seeding for each experiment is introduced into the wind tunnel upstream of the fan and the facility's flow conditioning and settling chamber, which provides a homogeneous seeding density across the test section. The illumination for the experiments is provided by an Innolas Spitlight Compact 400 Nd:YAG system that generates a light sheet on a streamwise wall-normal plane, which is projected upstream through the working section (see figure 2(b)). The mirror in the flow required for this configuration is 2.5 m (approximately 30δ) downstream of the surface transition. Hotwire surveys indicate that the presence of the mirror in the flow has no upstream effect on the flow.

Because multiple camera positions are used in the present experiments to construct a

General parameters	
Flow medium	Air
Seeding	Polyamide particles
Particle size	$\approx 1-2\,\mu$m
Acquisition frequency	1 Hz
Laser sheet thickness	≈ 1 mm ($\sim 30\nu/u_\tau$)
Flow parameters	
Reynolds number	$Re_\tau \approx 3500$
Freestream velocity	$U_\infty \approx 15$ m/s
PIV/PTV parameters	
Number of images	600
Sensor resolution	4008×2672 pixels
Image pixel size	≈ 12 µm/pixel
Field of view ($x \times z$)	≈ 0.05 m $\times$ 0.03 m
Interrogation size (PIV pass)	128×8 pixels
Overlap (PIV pass)	75%
Interrogation size (PTV pass)	4×4 pixels

Table 2: Summary of parameters for the PTV experiments

non-simultaneous wider streamwise FOV, a calibration procedure is essential to stitch the time-averaged statistics from the different camera positions together and also to account for image distortions. In the present experiments, we employ a calibration target that spans the entire extent of the FOV, which has been proven to work well for multi-camera large-FOV experiments (see de Silva et al. (2012, 2014)). For the present experiments the calibration target is composed of dotted pattern with a diameter of 1mm and have spacing between dots of 2.5mm in the $x-$ and $z-$ direction. A third order polynomial surface is fitted to the pixel location of the dots, which enables us to apply a pixel-to-real space conversion by mapping the pixel positions to real space coordinates within the wind tunnel.

The experimental image-pairs are processed using an in-house PIV/PTV package developed at the University of Melbourne (de Silva et al., 2014). For the present study, the images are first pre-processed using a conventional PIV cross-correlation algorithm, with multigrid (Willert, 1997) and window deformation (Scarano, 2001). Thereafter, a particle tracking pass is executed to track individual particles based on an initial estimate from the PIV pass (Cowen and Monismith, 1997). For the PIV processing vector validation is performed using a median filter (Westerweel and Scarano, 2005) and to validate the particle tracks in PTV thresholds are applied to the correlation coefficient and the size of the detected particles (Adrian and Westerweel, 2011). We note, due to the small interrogation window size (4×4 pixles) used in the PTV pass, velocity information can be obtained closer to the wall compared to the PIV pass (see figure 2c-d). Further, the wall-normal location of the PTV database is refined to subpixel accuracy by correlating the near wall particles and their reflections on a frame-by-frame basis. A summary of the parameters of the PTV databases is detailed in table 2.

2.2 Hotwire anemometry

To complement the PTV measurements, hotwire anemometry are acquired using a modified Dantec 55P15 boundary-layer-type probe equipped with a 2.5 µm diameter platinum Wollaston wire with a length-to-diameter ratio that exceeds 200 (Ligrani and Bradshaw, 1987). The

hotwire is operated by an in-house Melbourne University Constant Temperature Anemometer (MUCTA) at an over-heat ratio of 1.8 and sampled at 30 kHz for 150 seconds at each wall-normal location. In the present work, boundary layer profiles are taken at $\hat{x}$ = 10, 30, 60, 90, 180 and 360 mm (● symbols in figure 2), corresponding to $\hat{x}/\delta = 0.11, 0.34, 0.68, 1.0, 2.0, 4.1$, where $\hat{x} = 0$ is the location of the rough-to-smooth transition. Each profile consists of 50 logarithmically spaced measurement locations in the wall-direction from $z \approx 0.3$mm to $z/\delta \approx 2$. All measurements are acquired at a nominal freestream velocity of $U_\infty \approx 15$ m/s.

2.3 Oil film interferometry

The wall-shear stress τ_w is also directly measured using oil film interferometry (OFI), which is one of the few methods available for a direct measurement at the surface with the required streamwise resolution to capture the rapid evolution following the rough-to-smooth transition. The technique measures the thinning rate of an oil film as it is being acted upon by the shear near the wall, which in turn permits an accurate measure of the mean wall-shear stress. The thickness of a typical oil film is in the order of micrometres, which can be measured by the fringe pattern originated from the interference of light reflected from the top and from the bottom of the oil film. Moreover, the technique utilises inexpensive equipment, which includes a consumer camera and monochromatic light source (Zanoun et al., 2003; Fernholz et al., 1996).

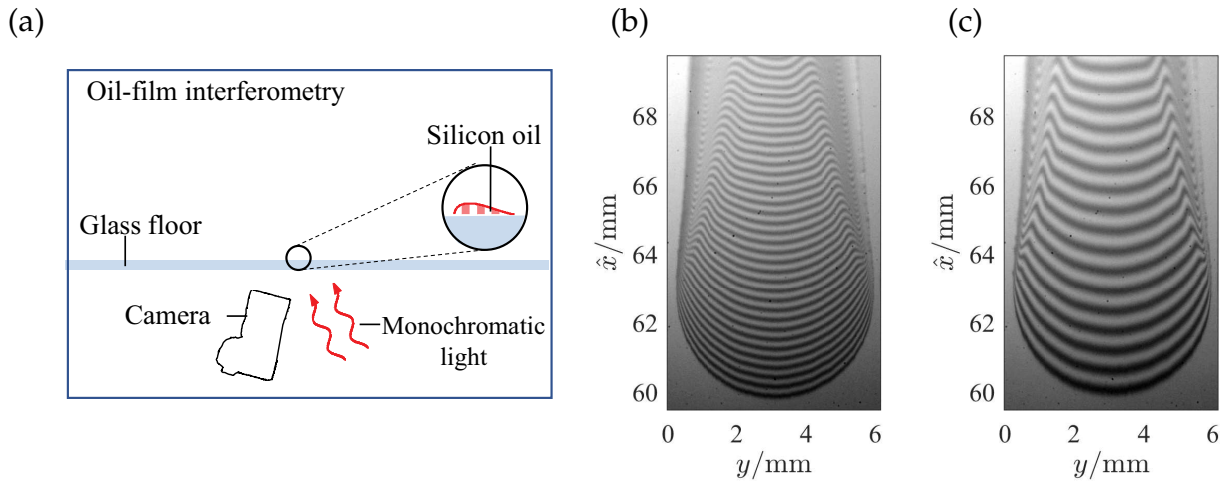

Figure 3: (a) Illustration of the OFI experimental setup. (b) and (c) are the first and last OFI image in the sequence obtained at $\hat{x} \approx 60$mm. The time interval between these two images is 495 s. Both images have been converted from pixel space to real space using a calibration process similar to that used in the PTV experiments.

The experimental configuration is illustrated in figure 3(a), where a silicon oil droplet is placed on a clear glass surface. The oil droplet is illuminated using a monochromatic light source from a sodium lamp and the interference pattern is captured using a Nikon D800 DSLR camera equipped with a 105mm AF Micro NIKKOR lens and a Sigma APO EX DG 2× teleconverter, which is mounted underneath the working section. Prior to the OFI measurements, the viscosity ν_{oil} of the oil is calibrated as a function of temperature T_{oil} using a constant temperature water bath and an Ubbelohde viscometer to obtain an exponential relationship, where $\nu_{oil} = Ae^{\alpha T_{oil}}$ (Ng et al., 2007). In a similar fashion to the PTV measurements, the FOV of the OFI measurements is calibrated with the same calibration target with 2.5 mm dot spacing, providing a precise conversion from image to real space.

For each OFI database, 100 images are captured with a time interval of five seconds between images. Figure 3(b) and (c) are the first and last image from one such image sequences acquired at $\hat{x} \approx 60$mm. For the present measurements, the resolution ranges from ≈ 100 pixels/fringe to ≈ 200 pixels/fringe, from the first to the last image, respectively to ensure that all the fringe patterns are fully resolved. The image sequences are then processed using an FFT based algorithm (Ng et al., 2007) to extract the fringe spacing of the interferograms. More specifically, following Ng et al. (2007) the signal is zero-padded to improve the dominant frequency estimation. Thereafter, a linear trend is fitted to the extracted fringe spacing of the interferograms versus time to evaluate the wall shear stress, τ_w. It should be noted that by performing FFT across the entire oil-film in the FOV, C_f is assumed to be constant within the FOV in each measurement which is known to vary after a rough-to-smooth transition, however, our findings confirm a variation of less than 1.5% (see figure 5) is expected within one centimetre in the streamwise direction (~typical extent of the oil film coverage in an image) for $\hat{x}/\delta > 0.3$.

3. Results

To begin with, we examine the wall-normal profiles of the mean streamwise velocity $\overline{U}$, from the hotwire database (figure 4a). Here, $\hat{x}$ corresponds to the distance downstream of the rough-to-smooth surface change. For the hotwire databases due to the lack of velocity signals in the near-wall region, U_τ has been estimated from a fit in the buffer region ($10 \lesssim z^+ \lesssim 30$). A least squares fit is performed between $\overline{U}^+$ from the experiments and a reference smooth-walled DNS database (Sillero et al., 2013). Further, due to the uncertainty associated with the precise wall-normal location of the hotwire measurements a wall-normal shift is included as a free parameter in the fit. Although the hotwire results for $\overline{U}^+$ (see figure 4a) exhibit good collapse in the buffer region ($10 \lesssim z^+ \lesssim 30$) to the canonical case (dashed line) as demanded by the buffer fit method, the quality of agreement in the near-wall region cannot be assessed due to a lack of near wall data.

Figure 4(b) presents $\overline{U}^+$ from the PTV database, where a more direct estimate of τ_w (hence U_τ) is accessible. More specifically, over a smooth walled surface, we are able to compute U_τ using a least squares fit in the viscous sublayer ($z^+ \lesssim 4$) following

$$U_\tau = \sqrt{\frac{\tau_w}{\rho}} = \sqrt{\nu \frac{\partial \overline{U}}{\partial z}}, \tag{1}$$

where ν is the kinematic viscosity. The results exhibit clear evidence that U_τ (and hence $\overline{U}$) estimated from the buffer and viscous sublayer region differs substantially. Therefore, this discrepancy highlights that the buffer region is yet to recover to an equilibrium state to the new surface conditions, and thus provides a poor estimate of the wall-shear stress (and hence U_τ) immediately after the rough-to-smooth transition.

Figure 5 presents the skin friction coefficient, C_f, downstream of the rough-to-smooth transition from all the experimental databases. We note, results from the PTV and OFI methods are measured directly from the near-wall velocity gradient deep in the viscous sublayer, while the hotwire databases use a buffer fit in the range $10 < z^+ < 30$ (red symbols). The results confirm that even beyond $\hat{x}/\delta > 1$ downstream of the transition, the magnitude of C_f at matched flow conditions exhibits a more gradual recovery as a function of $\hat{x}$ when estimated away from the wall (e.g. buffer fits), as compared to estimates evaluated closer to

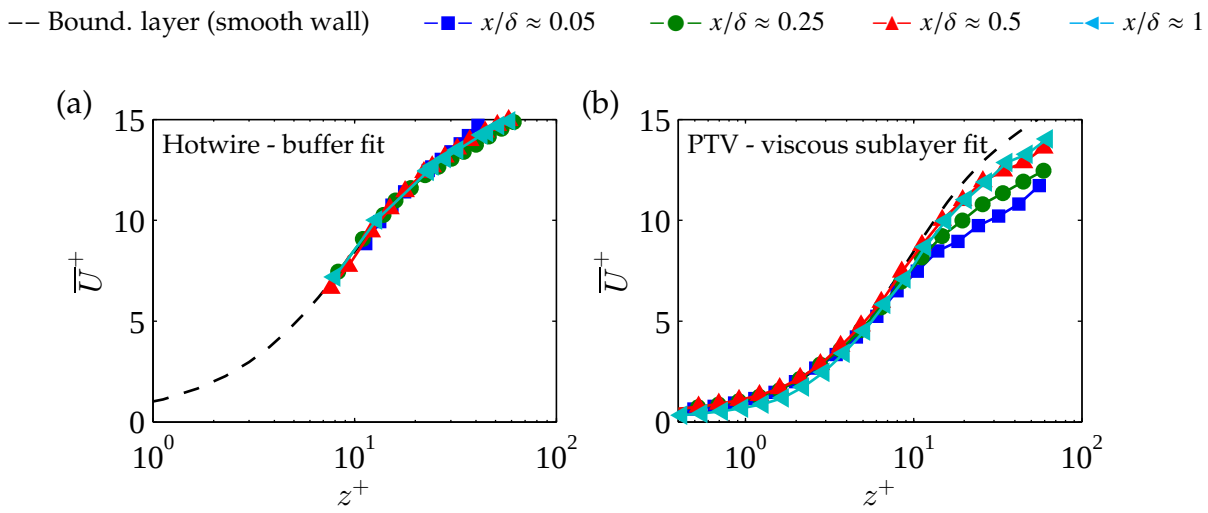

Figure 4: Mean flow statistics from Hotwire and PTV experimental data at $Re_\tau \approx 3500$. Normalisation is by friction velocity, U_τ, estimated from a fit to the (a) buffer and (b) viscous sublayer regions, and x corresponds to the streamwise distance from the rough-to-smooth transition. The black dashed line corresponds to a reference smooth walled boundary layer DNS database at $Re_\tau \approx 2500$ (Sillero et al., 2013).

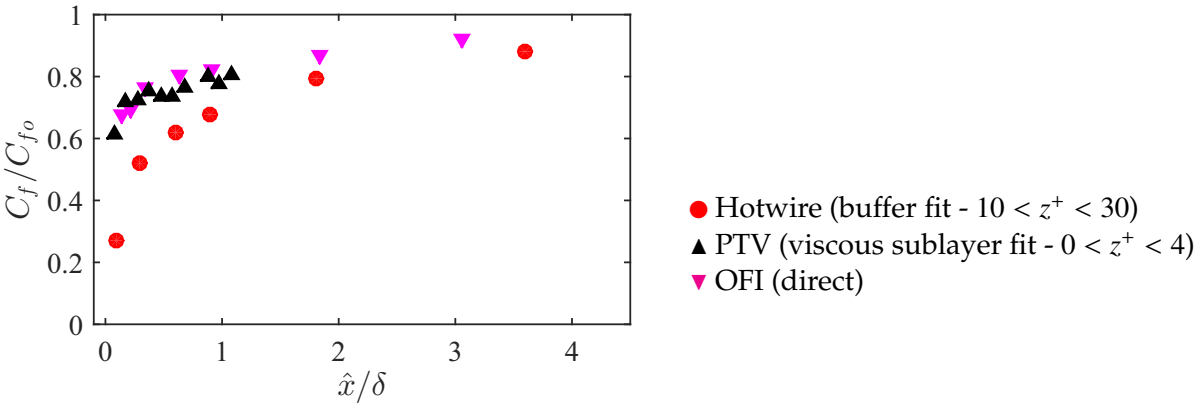

Figure 5: Coefficient of friction, C_f, estimates from the Hotwire, OFI and PTV experimental data at $Re_\tau \approx 3500$. Normalisation is by C_{fo}, which correspond to the last measured magnitude of C_f from the OFI database at $\hat{x}/\delta \approx 10$.

the wall (e.g viscous sublayer - PTV database) or at the wall (e.g. OFI). These discrepancies are likely to play a significant role in the wide range of recovery trends reported for C_f in past works Loureiro et al. (2010). Further, our findings confirm that high-magnification PTV techniques are more suited to measuring the wall shear stress after a sudden change in surface conditions, as compared to more established techniques that rely on assumed velocity profiles further from the wall (Clauser technique, buffer fits).

Although not reproduced here for brevity, we examine the same statistics using a direct numerical simulation database (DNS) of a rough-to-smooth transition, where a direct measure of the wall-shear stress τ_w is available. In doing so, we confirm that the mean flow in the buffer region and beyond, once normalised by U_τ exhibits poor agreement even after several boundary layer thickness downstream of the transition, indicating that these regions are yet to recover to an equilibrium state to the new wall conditions. As a consequence, any

estimate of τ_w (hence U_τ) obtained from the buffer region or above will be compromised.

5. Conclusions

This work presents a systematic study on estimating the wall-shear stress τ_w after a sudden change in surface conditions from a rough-to-smooth wall. To this end, a unique collection of experimental databases are examined that have access to both 'direct' and 'indirect' measures of τ_w. Our results reveal that the mean flow above the viscous sublayer ($z^+ \gtrsim 4$) only recovers to an equilibrium state to the new local smooth-wall conditions after several boundary layer thicknesses downstream of the rough-to-smooth transition. Based on these findings, conventional 'indirect' techniques that only have access to velocity information above the viscous region are shown to consistently underestimate the magnitude of τ_w immediately after a rough-to-smooth transition. On the other hand, techniques such as near-wall PIV / PTV are shown to be well-suited for an accurate measure of τ_w immediately after a rough-to-smooth transition. These results are also confirmed by utilising a direct numerical simulation database with a comparable rough-to-smooth surface change.

Acknowledgements

The authors gratefully acknowledge support from the Australian Research Council

References

Adrian, R. J. and Westerweel, J. *Particle Image Velcimetry*. Cambridge University Press, 2011.

Antonia, R. A. and Luxton, R. E. The response of a turbulent boundary layer to a step change in surface roughness. part 2. rough-to-smooth. *J. Fluid Mech.*, 53(4):737–757, 1972.

Bradley, E. F. A micrometeorological study of velocity profiles and surface drag in the region modified by a change in surface roughness. *J. Roy. Met. Soc.*, 94(401):361–379, 1968.

Chamorro, L. P. and Porté-Agel, F. Velocity and surface shear stress distributions behind a rough-to-smooth surface transition: a simple new model. *Bound. layer Metrol.*, 130(1):29–41, 2009.

Cowen, E. A. and Monismith, S. G. A hybrid digital particle tracking velocimetry technique. *Exp. Fluids*, 22(3):199–211, 1997.

de Silva, C. M., Chauhan, K. A., Atkinson, C. H., Buchmann, N. A., Hutchins, N., Soria, J., and Marusic, I. Implementation of large scale PIV measurements for wall bounded turbulence at high Reynolds numbers. In 18^{th} *Aust. Fluid Mech. Conf.*, volume 18, pages 308–311, Launcheston, Australia, 2012.

de Silva, C. M., Gnanamanickam, E., Atkinson, C., Buchmann, N. A., Hutchins, N., Soria, J., and Marusic, I. High spatial range velocity measurements in a high Reynolds number turbulent boundary layer. *Phys. Fluids*, 26(2):025117, 2014.

Fernholz, H., Janke, G., Schober, M., Wagner, P., and Warnack, D. New developments and applications of skin-friction measuring techniques. *Measurement Science and Technology*, 7(10):1396, 1996.

Garratt, J. R. The internal boundary layer - A review. *Boundary-Layer Meteorology*, 50(1-4):171–203, 1990.

Hanson, R. E. and Ganapathisubramani, B. Development of turbulent boundary layers past a step change in wall roughness. *J Fluid Mech.*, 795:494–523, 2016.

Kähler, C. J., Scharnowski, S., and Cierpka, C. High resolution velocity profile measurements in turbulent boundary layers. In 16^{th} *Int. Symp. App. Laser Tech. Fluid Mech., Lisbon, Portugal, 09-12 July*, 2012.

Kevin, Nugroho, B., Monty, J. P., Hutchins, N., Pathikonda, G., Barros, J. M., and Christensen, K. T. Dissecting a modified turbulent boundary layer using particle image velocimetry. In *7th Aust. Conf. Laser Diag. Fluid Mech. Comb.*, 2015.

Ligrani, P. M. and Bradshaw, P. Spatial resolution and measurement of turbulence in the viscous sublayer using subminiature hot-wire probes. *Exp. Fluids*, 5(6):407–417, 1987.

Loureiro, J. B. R., Sousa, F. B. C. C., Zotin, J. L. Z., and Freire, A. P. S. The distribution of wall shear stress downstream of a change in roughness. *Int. J. Heat Fluid Flow*, 31(5):785–793, 2010.

Ng, H. C. H., Marusic, I., Monty, J. P., Hutchins, N., and Chong, M. S. Oil film interferometry in high

Reynolds number turbulent boundary layers. In *16th Aust. Fluid Mech. Conf.*, pages 807–814. School of Engineering, The University of Queensland, 2007.
Nugroho, B., Hutchins, N., and Monty, J. P. Large-scale spanwise periodicity in a turbulent boundary layer induced by highly ordered and directional surface roughness. *Int. J. Heat Fluid Flow*, 41:90–102, 2013.
Rao, K. S., Wyngaard, J. C., and Coté, O. R. The structure of the two-dimensional internal boundary layer over a sudden change of surface roughness. *J. Atm. Sci.*, 31(3):738–746, 1974.
Scarano, F. Iterative image deformation methods in PIV. *Meas Sci Tech.*, 13:R1–19, 2001.
Shir, C. C. A numerical computation of air flow over a sudden change of surface roughness. *J. Atm. Sci.*, 29(2):304–310, 1972.
Sillero, J. A., Jiménez, J., and Moser, R. D. One-point statistics for turbulent wall-bounded flows at Reynolds numbers up to $\delta^+ = 2000$. *Phys. Fluids*, 25(10):105102, 2013.
Tropea, C., Yarin, L. A., and Foss, J. F. *Springer Handbook of Experimental Fluid Mechanics*. Springer, Heidelberg, 2007.
Westerweel, J. and Scarano, F. Universal outlier detection for PIV data. *Exp. Fluids*, 39(6):1096–1100, 2005.
Willert, C. Stereoscopic digital particle image velocimetry for application in wind tunnel flows. *Meas. Sci. Tech.*, 8(12):1465, 1997.
Zanoun, E. S., Durst, F., and Nagib, H. Evaluating the law of the wall in two-dimensional fully developed turbulent channel flows. *Physics of Fluids*, 15(10):3079–3089, 2003.